Investigation of the alignment mechanism and loss of collectivity in ^{135}Pm

F. S. Babra,[1] S. Jehangir,[1] R. Palit,[1] S. Biswas,[1] B. Das,[1] S. Rajbanshi,[2] G. H. Bhat,[3,4] J. A. Sheikh,[5] Biswajit Das,[1] P. Dey,[1] U. Garg,[6] Md. S. R. Laskar,[1] C. Palshetkar,[1] S. Saha,[1] L. P. Singh,[1] and P. Singh[1]

[1]*Department of Nuclear and Atomic Physics, Tata Institute of Fundamental Research, Mumbai 400005, India*
[2]*Department of Physics, Presidency University, Kolkata 700073, India*
[3]*Department of Physics, SP College Srinagar, Jammu and Kashmir 190001, India*
[4]*Department of Physics, Cluster University Srinagar, Jammu and Kashmir, Srinagar, Goji Bagh 190008, India*
[5]*Department of Physics, University of Kashmir, Hazratbal, Srinagar 190006, India*
[6]*Physics Department, University of Notre Dame, Notre Dame, Indiana 46556, USA*

(Received 6 September 2020; revised 1 November 2020; accepted 7 January 2021; published 21 January 2021)

High-spin excited states of ^{135}Pm have been investigated using the ^{107}Ag(^{32}S, $2p2n$) reaction at 145-MeV beam energy. Three negative-parity bands have been investigated up to ∼9.0-, 7.6-, and 6.9-MeV excitation energies with spin parities $(55/2^-)$, $(49/2^-)$, and $(47/2^-)$ $\hbar$, respectively. The experimental results have been interpreted using the triaxial projected shell model. It is shown that the observation of the parallel band structures can be explained in terms of crossing of two s bands with the yrast band, which is a rare phenomenon for an odd-A nucleus. Further, the lifetimes of levels in yrast band have been extracted using Doppler shift attenuation method. The evaluated $B(E2)$ values of yrast states show the loss of collectivity at higher spin, attributed to the alignment process.

DOI: 10.1103/PhysRevC.103.014316

I. INTRODUCTION

Neutron-deficient nuclei in the $A \sim 130$ region occupy a unique place in the nuclear periodic table to shed light on various nuclear structure phenomena. In this region, neutrons and protons occupy the same $h_{11/2}$ intruder orbital and the evolution of their shapes with angular momentum depicts fascinating dynamics [1,2]. The proton Fermi surface lies near the bottom of the $h_{11/2}$ subshell, whereas the neutron Fermi surface lies in the vicinity of the upper part of the $h_{11/2}$ subshell. Investigation of proton and neutron alignments for the rotational bands in these nuclei remains a subject of great interest due to their importance in shape evolution as well as being drivers of different excitation modes. A recent study reported a shape change for the yrast band due to particle alignment in ^{136}Sm [3], an isotone of ^{135}Pm. The sharp drop in the $B(E2)$ values above $I^\pi = 15/2^-$ in ^{135}Pm reported in the previous work [4] is similar to the behavior observed in ^{127}La [5]. This feature has not been explained by any model calculations and merits further experimental as well as theoretical investigation. In particular, more lifetime data are required for the higher-spin states in this nucleus to probe the evolution of collectivity. Several studies have been undertaken to understand the high-spin structural properties of many odd-A nuclei in this region [6–17]. Pm isotopes with $N \sim 74$ have significant γ softness [18] and has been predicted to have large shape changes [19] driven by alignment of high-j quasiparticles. Both proton and neutron pair alignments in ^{133}Pm, ^{135}Pm, and ^{137}Pm isotopes drive shape changes with increasing spin [16]. The alignment process for some of these nuclei has been found to be much more complicated than previously thought [20]. Of particular interest is the nature of alignment of yrast bands in odd Pr and Pm isotopes, which are built on a decoupled $h_{11/2}$ proton. While for lighter isotopes like ^{131}Pm, the self-consistent model predicts that the alignment of a pair of $h_{11/2}$ neutrons dominates over $h_{11/2}$ proton pair, their role changes for isotopes heavier than ^{135}Pm. Though the model explains the alignment and dynamic moment of inertia for ^{135}Pm [20], an elaborate discussion of the band-crossing and available transition strengths are required to understand the subtle process of alignment mechanism in ^{135}Pm and its effect on evolution of collectivity.

The present paper accounts for a detailed investigation of three negative-parity band structures in ^{135}Pm. Lifetime measurements were carried out to examine the yrast band structures. The results are discussed using the microscopic triaxial projected shell-model (TPSM) approach.

II. EXPERIMENTAL DETAILS

Two separate experiments were performed with Indian National Gamma Array facility at Tata Institute of Fundamental Research (TIFR), Mumbai, using the reaction ^{107}Ag(^{32}S, $2p2n$). The ^{32}S beam of 145-MeV energy was provided by Pelletron Linac facility at TIFR. In the first experiment, 1.2-mg/cm^2-thick ^{107}Ag target was used with ^{197}Au backing of thickness 12.5 mg/cm^2 to stop the recoiling nuclei. The emitted γ rays were detected using an array of 18 Compton-suppressed HPGe clover detectors arranged in the rings placed at angles (number of detectors) 23° (2), 40° (2), 65° (2),

90° (4), 115° (2), 140° (3), and 157° (3) with respect to the beam direction. In the second experiment, a self-supporting ^{107}Ag target of 0.95 mg/cm^2 thickness has been used and the measurement was carried out with the array of 11 Compton-suppressed HPGe clovers arranged at angles 23° (1), 90° (4), 140° (3), and 157° (3). Both ^{152}Eu and ^{133}Ba radioactive sources were used for measuring the energy calibration and relative photopeak efficiency of the clover detectors. Two- and higher-fold coincidence events were recorded using a fast digital data acquisition system based on the Pixie-16 module of XIA-LLC [21]. The time-stamped data were sorted using multiparameter coincidence search program developed at TIFR [22] to generate one-dimensional histograms, γ-γ matrix, and γ-γ-γ cube in RADWARE package [23] for the data analysis. The gated spectra with background subtraction were used to construct the level scheme.

The spins of the levels were assigned using directional correlation of oriented states (DCO), from the coincidence spectra of detectors at 90° and 157°. The DCO ratio is defined as [24]

$$R_{\mathrm{DCO}} = \frac{I^{\gamma_1}{}_{157^\circ}(G^{\gamma_2}{}_{90^\circ})}{I^{\gamma_1}{}_{90^\circ}(G^{\gamma_2}{}_{157^\circ})},$$

where I is the observed intensity of the transition and G is the gating transition. The DCO ratios of stretched dipole and quadrupole transitions are ∼0.5(1.0) and ∼1.0(2.0), respectively, for a pure quadrupole (dipole) gate.

The parities of the states were obtained by measuring the polarization asymmetry (Δ) given by [25]:

$$\Delta = \frac{a(E_\gamma)N_\perp - N_\parallel}{a(E_\gamma)N_\perp + N_\parallel},$$

using the 90° clover detectors as polarimeter [26,27]. Here $N_\parallel(N_\perp)$ is the number of γ transitions scattered parallel (perpendicular) to the reaction plane and $a(E_\gamma)$ is a correction factor for the parallel to perpendicular scattering asymmetry between the crystal pairs of a clover. The value of $a(E_\gamma)$ was obtained by fitting the polynomial $c + dE_\gamma$ as a function of energy (E_γ) of unpolarized photons emitting from ^{133}Ba–^{152}Eu sources. The values $c = 0.982(0.005)$ and $d = -2.38(2.50) \times 10^{-6}$ were found. The polarization asymmetry values of the transitions were then extracted following the construction of two asymmetric matrices with coincident events corresponding to parallel and perpendicularly scattered γ rays at 90° detectors. A positive value of Δ indicates electric nature of transition while negative value corresponds to magnetic nature [28].

III. DATA ANALYSIS AND RESULTS

A. Level scheme

The partial level scheme of ^{135}Pm, established from the present work, is presented in Fig. 1. The ordering of the γ rays is based on the coincidence relationships and relative photopeak intensities. The spin and parity assignments are based on R_{DCO} and Δ values. The level scheme has been modified and extended with the inclusion of 15 new transitions which are in red in Fig. 1. The γ-ray energies, relative intensities, polarization asymmetry values, multipolarities, DCO ratios, level

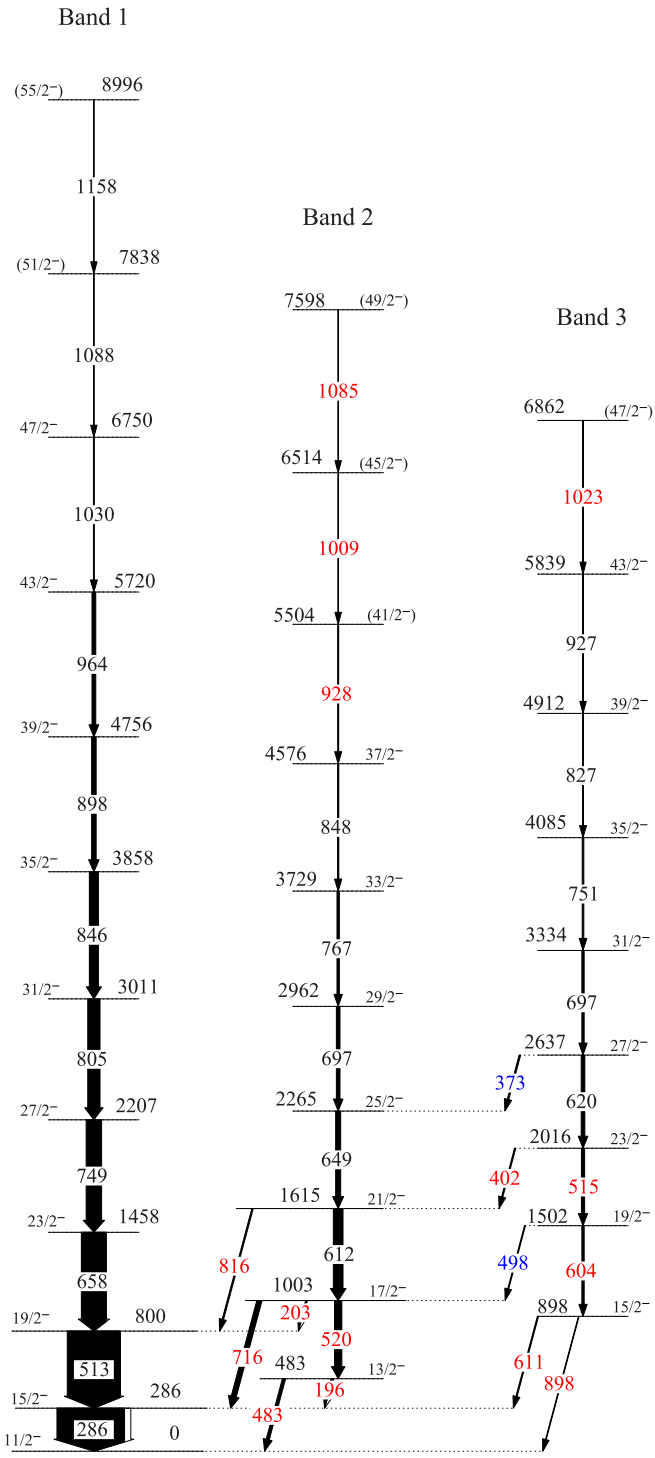

FIG. 1. Partial level scheme of ^{135}Pm consisting of negative-parity states obtained from the present work. The level energies are given relative to the $11/2^-$ state of Band 1. The new transitions are shown in red while the rearranged transitions are shown in blue. The arrow widths are proportional to the transition intensity and the white portion corresponds to the internal-conversion component. The energies of levels and gamma transitions given in keV are rounded off to the nearest integer values.

energies, and spin values associated with the negative-parity states are listed in Table I. Few significant modifications were

TABLE I. Excitation energies of the initial decaying levels (E_i), energies of γ rays (E_γ), initial to final states of the transitions, relative intensities (I_γ), $R_{\rm DCO}$ and polarization asymmetry (Δ) values for the negative-parity states of ^{135}Pm are listed. The level energies are given relative to the $11/2^-$ state of Band 1. The deduced multipolarities are also quoted in the last column based on $R_{\rm DCO}$ and Δ values. The uncertainties in the energies of γ rays are 0.2 keV for intense transitions ($I_\gamma > 50$) and 0.7 keV ($I_\gamma < 5$) for weak transitions. For transitions with intermediate intensities, the uncertainties in energies vary between 0.2 and 0.7 keV.

Band	E_i (keV)	E_γ (keV)	$I_i^\pi \rightarrow I_f^\pi$	I_γ	$R_{\rm DCO}$[a]	Δ	Multipolarity
1	286.5	286.5	$15/2^- \longrightarrow 11/2^-$	100	0.97(11)	0.06(3)	$E2$
	799.8	513.3	$19/2^- \longrightarrow 15/2^-$	77(5)	0.92(10)	0.05(1)	$E2$
	1457.8	658.0	$23/2^- \longrightarrow 19/2^-$	36.7(26)	1.01(10)	0.09(2)	$E2$
	2206.6	748.8	$27/2^- \longrightarrow 23/2^-$	22.2(16)	1.03(10)	0.12(2)	$E2$
	3011.5	804.9	$31/2^- \longrightarrow 27/2^-$	18.0(13)	0.96(10)	0.08(3)	$E2$
	3857.9	846.4	$35/2^- \longrightarrow 31/2^-$	12.8(9)	0.89(10)	0.07(5)	$E2$
	4756.2	898.3	$39/2^- \longrightarrow 35/2^-$	5.5(4)	1.04(11)	0.12(8)	$E2$
	5720.3	964.1	$43/2^- \longrightarrow 39/2^-$	2.86(20)	1.01(11)		$E2$
	6750.2	1029.9	$47/2^- \longrightarrow 43/2^-$	1.24(9)	0.86(11)		$E2$
	7838.2	1088.0	$(51/2^-) \longrightarrow 47/2^-$	0.56(9)			$(E2)$
	8996.5	1158.3	$(55/2^-) \longrightarrow (51/2^-)$	0.38(8)			$(E2)$
2	1002.8	520.0	$17/2^- \longrightarrow 13/2^-$	8.51(60)	0.92(13)	0.17(8)	$E2$
	1615.3	612.5	$21/2^- \longrightarrow 17/2^-$	14.1(10)	1.00(10)	0.09(3)	$E2$
	2264.8	649.5	$25/2^- \longrightarrow 21/2^-$	7.28(51)	1.07(12)	0.03(5)	$E2$
	2961.6	696.8	$29/2^- \longrightarrow 25/2^-$	5.32(39)	1.11(13)		$E2$
	3729.0	767.4	$33/2^- \longrightarrow 29/2^-$	5.23(37)	0.92(11)		$E2$
	4576.6	847.6	$37/2^- \longrightarrow 33/2^-$	3.66(26)	1.02(13)		$E2$
	5504.4	927.8	$(41/2^-) \longrightarrow 37/2^-$	1.51(11)			$(E2)$
	6513.8	1009.4	$(45/2^-) \longrightarrow (41/2^-)$	0.81(6)			$(E2)$
	7598.4	1084.6	$(49/2^-) \longrightarrow (45/2^-)$	0.31(7)			$(E2)$
$2 \rightarrow 1$	482.8	195.9	$13/2^- \longrightarrow 15/2^-$	2.78(20)	0.44(5)		$E2/M1$
	482.8	482.8	$13/2^- \longrightarrow 11/2^-$	6.56(30)	0.48(13)	−0.07(7)	$E2/M1$
	1002.8	202.6	$17/2^- \longrightarrow 19/2^-$	1.61(11)			
	1002.8	716.3	$17/2^- \longrightarrow 15/2^-$	6.33(45)	0.47(6)	−0.02(4)	$E2/M1$
	1615.3	815.5	$21/2^- \longrightarrow 19/2^-$	1.98(14)	0.55(6)	−0.07(14)	$E2/M1$
3	1501.8	604.0	$19/2^- \longrightarrow 15/2^-$	2.84(20)	1.10(13)	0.16(8)	$E2$
	2016.5	514.7	$23/2^- \longrightarrow 19/2^-$	4.12(29)	0.99(13)		$E2$
	2636.8	620.3	$27/2^- \longrightarrow 23/2^-$	3.51(23)	1.02(11)	0.14(4)	$E2$
	3334.0	697.2	$31/2^- \longrightarrow 27/2^-$	3.72(26)	0.96(10)		$E2$
	4084.8	750.8	$35/2^- \longrightarrow 31/2^-$	2.27(16)	0.83(10)		$E2$
	4912.1	827.3	$39/2^- \longrightarrow 35/2^-$	1.85(13)	0.93(10)		$E2$
	5839.4	927.3	$43/2^- \longrightarrow 39/2^-$	0.88(17)	0.99(21)		$E2$
	6862.4	1023.0	$(47/2^-) \longrightarrow 43/2^-$	0.40(4)			$(E2)$
$3 \rightarrow 1$	897.8	610.9	$15/2^- \longrightarrow 15/2^-$	1.42(12)	0.60(8)		$E2/M1$
	897.8	897.8	$15/2^- \longrightarrow 11/2^-$	1.25(10)	0.96(13)		$E2$
$3 \rightarrow 2$	1501.8	498.0	$19/2^- \longrightarrow 17/2^-$	2.6(2)			$(E2/M1)$
	2016.5	402.2	$23/2^- \longrightarrow 21/2^-$	1.55(11)			$(E2/M1)$
	2636.8	373.4	$27/2^- \longrightarrow 25/2^-$	1.29(12)	0.65(7)	−0.08(10)	$E2/M1$

[a] $R_{\rm DCO}$ values are obtained from the gate on $E2$ transitions.

being implemented for the level scheme over the available earlier results reported in Ref. [29] and are discussed in detail below.

The cascade of stretched $E2$ transitions with energies of 286, 513, 658, 749, 805, 846, 898, 964, 1030, 1088, and 1158 keV form the yrast band for ^{135}Pm. From the Nilsson systematics, this band has been assigned $\pi h_{11/2}$ configuration at low spin [29]. Based on the linking transitions which feed to the yrast band from a positive-parity band [29], the bandhead of the yrast $\pi h_{11/2}$ band has been placed 69 keV above the $I^\pi = (5/2^+)$ state whose relative position with respect to the actual ground state remains uncertain. The $\pi h_{11/2}$ yrast band was observed up to $I^\pi = (55/2^-)$ at an excitation energy, $E_{\rm exc} = 8.996$ MeV with respect to the $I^\pi = 11/2^-$ state and indicated as Band 1 in Fig. 1. All the levels energies in Fig. 1, are given relative to the $11/2^-$ state of Band 1. It has been confirmed and is in well agreement with the results reported in Ref. [20]. The coincidence spectrum used to identify γ-ray peaks of the yrast band is shown in Fig. 2(a). In the present discussion, other two negative-parity bands are designated as Band 2 and Band 3. Some of the transitions in these two bands were previously assigned to two positive-parity bands in Ref. [29]. The cascade of γ rays with 520-, 612-, 649-, 697-, 767-, 848-, 928-, 1009-, and 1085-keV energies has been

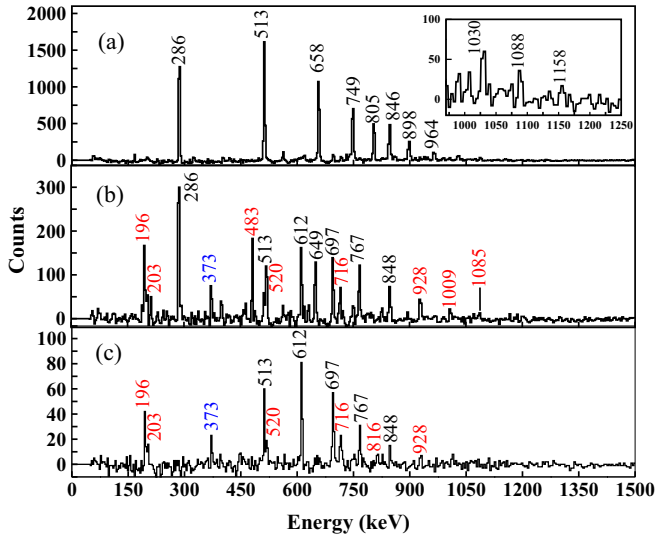

FIG. 2. Spectrum obtained from the double gate on (a) A/B, where A is the list gate of 286, 513, 658 keV and B is the list gate of 749, 805, 846, 898, 964, and 1030 keV; (b) C/C, where C is the list gate of 520, 612, 649, 697, and 767 keV; and (c) 286 and 649 keV. The new and rearranged transition energy values are marked red and blue, respectively.

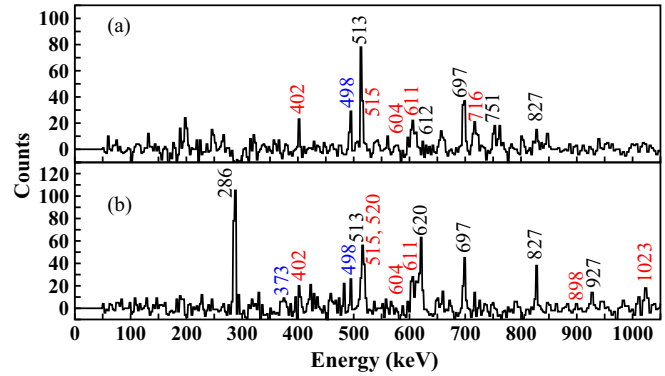

FIG. 3. Spectrum obtained from the (a) double gate on 286/620 keV and (b) sum of L/751-keV and L/927-keV double gates, where L is the list gate of 604, 620, 697, and 827 keV. The new and rearranged transition energy values are marked red and blue, respectively.

assigned as Band 2 (see Fig. 1) extending up to $I^{\pi} = (49/2^{-})$ and $E_{\rm exc} = 7.598$ MeV with respect to the $I^{\pi} = 11/2^{-}$. It decays to yrast band through 196-, 203-, 483-, 716-, and 816-keV transitions. $R_{\rm DCO}$ and Δ values of interconnecting 483-, 716-, and 816-keV transitions suggest $M1{+}E2$ multipolarity which is consistent with $\Delta I = 1$ and no parity change. Spectra containing both the interlinking transitions as well as intraband transitions of Band 2 are shown in Figs. 2(b) and 2(c).

Band 3 is observed as a cascade of $\Delta I = 2$ transitions from $I^{\pi} = 15/2^{-}$ to $I^{\pi} = (47/2^{-})$ as shown in Fig. 1. It decays to Band 2 via 498-, 402-, and 373-keV γ rays. They were incorrectly placed in prior work [29] except 402-keV transition which is a new finding in the present work. It also decays to yrast band via 611- and 898-keV as evident from Fig. 1. The 498-keV transition was incorrectly placed in Ref. [29] and is found to be decaying from $I^{\pi} = 19/2^{-}$ of Band 3 to $I^{\pi} = 17/2^{-}$ of Band 2. Addition of new 604-, 515-, and 1023-keV transitions extends Band 3 up to $E_{\rm exc} = 6.862$ MeV with respect to the $I^{\pi} = 11/2^{-}$. The $M1{+}E2$ character of the 373-keV transition was deduced from the experimental $R_{\rm DCO} = 0.65(7)$ and $\Delta = -0.08(10)$ values which affirms the negative parity of levels in band 3. Spectra showing transitions of Band 3 are shown in Figs. 3(a) and 3(b).

B. Lifetime measurements

Doppler-broadened line shapes were observed for the excited states of Band 1 from $I^{\pi} = 23/2^{-}$ to $I^{\pi} = 39/2^{-}$. Lifetimes of these states were extracted using the LINESHAPE code developed by Wells and Johnson [30]. The shell-corrected Northcliffe and Schilling electronic stopping power and range [31] were used for the energy-loss calculations of the residual nuclei moving through the target backing. Monte Carlo simulations within the program were used to generate the history of velocity profiles of recoiling nuclei moving inside the target and backing. Angle specific velocity profiles, generated using the geometry of the detectors and the array, were used as input parameters [32] along with the energies of γ-ray transitions and side-feeding intensities. During the fitting process, side-feeding into each level was modelled as a cascade of five transitions having a fixed moment of inertia which is chosen to be close to the average value of the yrast band. The side-feeding intensity for each state except for $I^{\pi} = 23/2^{-}$ level in cascade were determined using the relative intensities of transitions in gated spectra. The topmost transition of the investigated band with observed shape was assumed to have a 100% side-feeding intensity, yielding an effective lifetime for the state.

To perform the line-shape analysis of 658-, 749-, 805-, 846-, and 898-keV transitions, angle-dependent E_{γ}-E_{γ} asymmetric matrices were used to construct the background subtracted coincidence spectra from various detector angles. Each of these asymmetric matrices contain γ rays from specific angle in one axis and its coincident gammas at any angles in the other axis. For the 658-keV, top gate was used while the bottom gates were used for the other transitions above the 658-keV transition. Theoretical line shapes from 23°, 40°, 65°, 90°, 115°, 140°, and 157° detectors were fitted simultaneously to extract the lifetimes. Statistical uncertainties in the extracted lifetimes, given in Table II, were obtained from

TABLE II. Experimental mean lifetimes and $B(E2)$ values for the yrast band (Band 1) excited states in ^{135}Pm.

γ Energy (keV)	I_i^{π} ($\hbar$)	τ (ps)	$B(E2)$ (e^2 b^2)
658.0	$23/2^{-}$	$1.16^{+0.09}_{-0.09}$	$0.57^{+0.05}_{-0.04}$
748.8	$27/2^{-}$	$0.53^{+0.04}_{-0.04}$	$0.65^{+0.05}_{-0.05}$
804.9	$31/2^{-}$	$0.34^{+0.03}_{-0.03}$	$0.71^{+0.07}_{-0.06}$
846.4	$35/2^{-}$	$0.37^{+0.04}_{-0.04}$	$0.51^{+0.06}_{-0.05}$
898.3	$39/2^{-}$	<0.31	>0.45

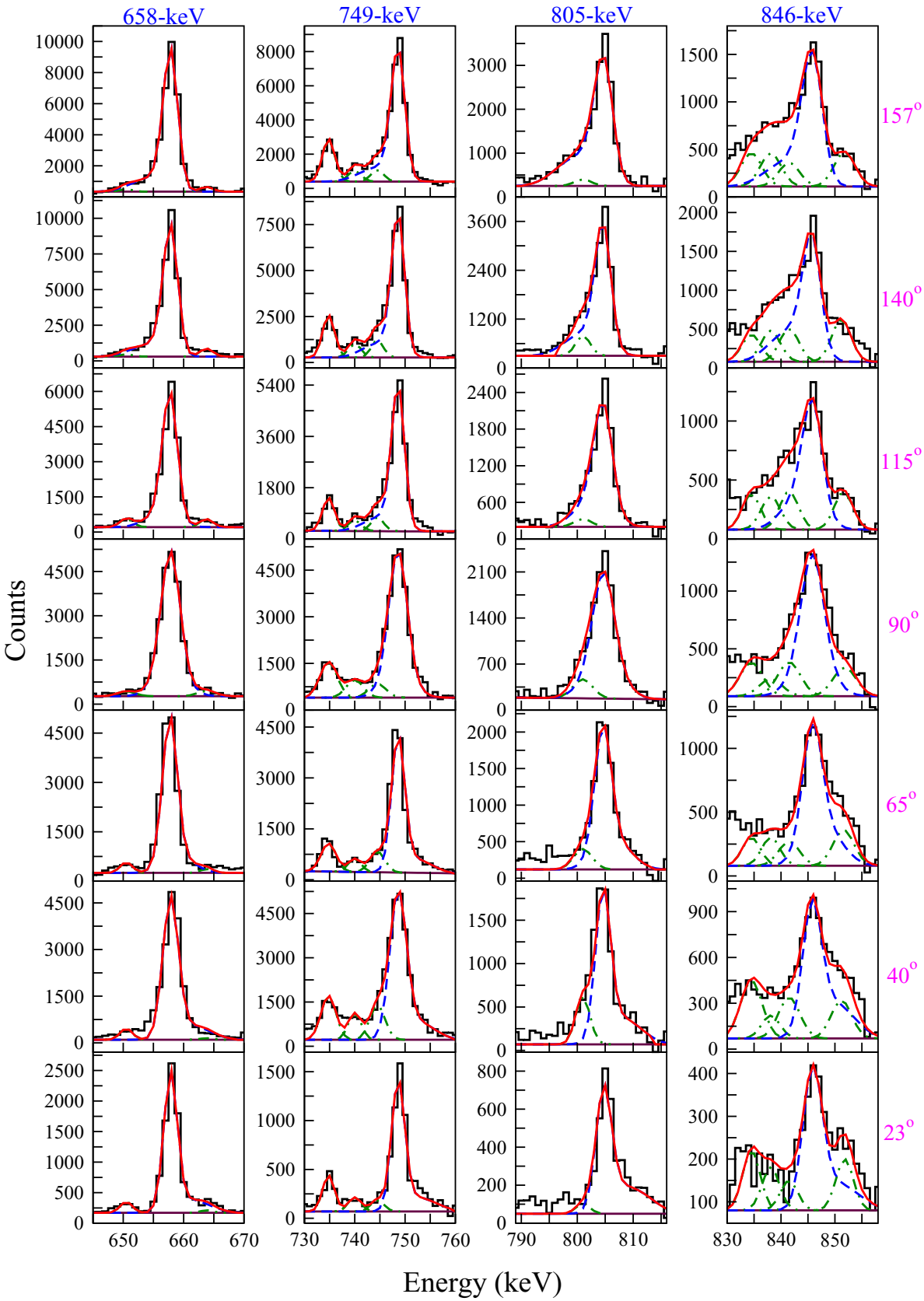

FIG. 4. The theoretically fitted line-shape spectra for 658-, 749-, 805- and 846-keV quadrupole transitions of the yrast band in ^{135}Pm. The, contaminant peaks, and total line shapes of the above-mentioned transitions are represented in dashed (blue), dot-dashed (green), and solid (red) lines, respectively.

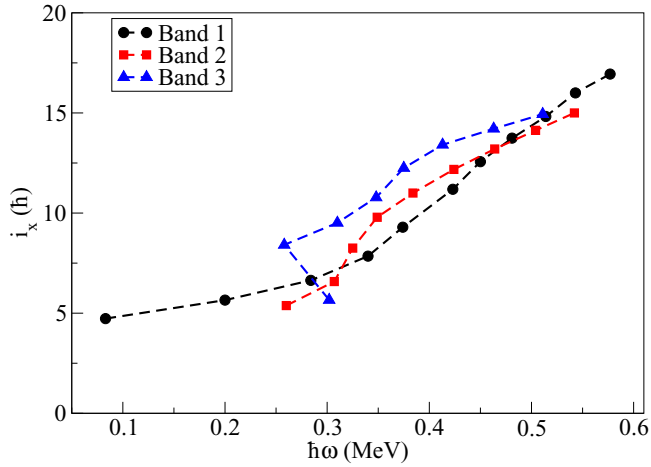

FIG. 5. Experimental alignment, i_x for the negative-parity bands in ^{135}Pm is plotted against the rotational frequency ($\hbar\omega$). Harris parameters $J_0 = 12.5\ \hbar^2\ \mathrm{MeV}^{-1}$ and $J_1 = 20\ \hbar^4\ \mathrm{MeV}^{-3}$ were used.

the behavior of the χ^2 in the vicinity of the minimum by a statistical method using the MINOS program [33,34]. The contribution from the systematic errors due to the stopping power calculations was not included and can be as large as 15%. The fitted lineshapes are shown in Fig. 4.

The experimental $B(E2)$ transition strengths were deduced from the experimental lifetimes measured using Doppler shift attenuation method (DSAM) from the relation

$$B(E2) = \frac{0.0816 B_r(E2)}{{E_\gamma}^5 \tau [1 + \alpha_t(E2)]}, \quad \text{in } (e\,\mathrm{b})^2 \qquad (1)$$

wherein E_γ is the transition energy in MeV, $B_r(E2)$ is the $E2$ branching ratio, τ is the mean lifetime in ps of the decaying level, and α_t is total internal conversion coefficient of the transition. The measured lifetime and $B(E2)$ values are presented in Table II. The values of $B_r(E2)$ are taken as unity while α_t are assumed to be zero which are good approximations for the stretched $E2$ transitions under consideration.

IV. DISCUSSION

The three negative-parity bands observed in ^{135}Pm and their decay pattern are similar to that observed in ^{133}Pm [15]. For the case of heavier ^{137}Pm isotope, only one well developed negative-parity band based on $\pi h_{11/2}$ orbital has been identified [35]. Band 1 in ^{135}Pm is based on the signature $\alpha =$ -1/2 component of $\pi[541]\ 3/2^-$ Nilsson orbital originating from $h_{11/2}$ proton subshell. Band 2 exhibits the character of the unfavored signature partner, $\alpha = +1/2$, beginning at a level energy of 483 keV with $I^\pi = 13/2^-$. A large signature splitting is expected between these partner bands as the proton fermi surface lies around lower $\Omega = 3/2$ orbital of $h_{11/2}$ subshell. Similar configurations have been assigned for two of the negative-parity bands in ^{133}Pm [15]. However, the configuration of the third negative-parity band in ^{133}Pm is not clear. The experimental alignment of rotational bands are plotted verses rotational frequency for ^{135}Pm in Fig. 5. A gradual increase in alignment of yrast band in ^{131}Pm, upbend

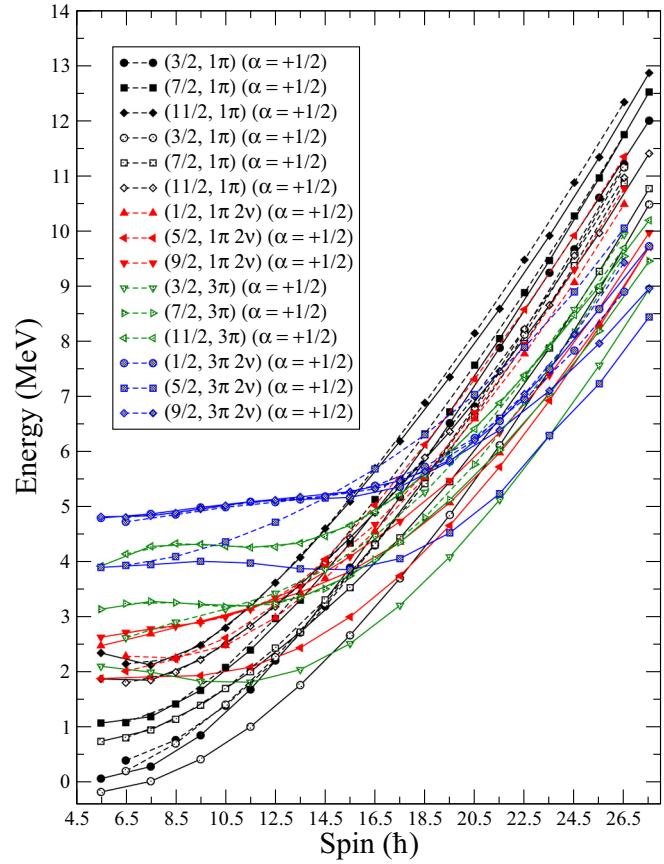

FIG. 6. TPSM projected energies, before band mixing, of negative-parity states for ^{135}Pm. Bands are labeled by $(K, \#)$ that designate the quasiparticle states with K quantum number and # the number of quasiparticles. For instance, $(3/2,\ 1\pi)$, $(7/2,\ 1\pi)$, $(11/2,\ 1\pi)$ correspond to the $K = 3/2, 7/2, 11/2$ one-proton quasiparticle state. The three-quasiparticle states with configurations $(1/2,\ 1\pi 2\nu)$, $(5/2,\ 1\pi 2\nu)$, $(9/2,\ 1\pi 2\nu)$, $(3/2,\ 3\pi)$, $(7/2,\ 3\pi)$, $(11/2,\ 3\pi)$ corresponding to the $K = 1/2, 5/2, 9/2, 3/2, 7/2, 11/2$ include two-neutron and two-proton configurations on the basic one-proton configuration. The excited $K = 1/2, 5/2, 9/2$ resulting from projection of three-quasiprotons and two-quasineutrons are denoted by $(1/2, 3\pi 2\nu)$, $(5/2, 3\pi 2\nu)$, $(9/2, 3\pi 2\nu)$ respectively. Because of large signature splitting, bands are separated into favored signature partner (labelled as $\alpha = -1/2$) and unfavored signature partner (labelled as $\alpha = +1/2$). The solid curves represent the $\alpha = -1/2$ states with same legend symbols and quasiparticle states as that of $\alpha = +1/2$ states plotted in dashed curves. The first crossing at $I = 31/2$ is due to $(3/2, 3\pi)$ aligned configuration that forms the yrast-band configuration. The second crossing at about $I = 43/2$ is due to $(5/2, 3\pi 2\nu)$ 5-quasiparticle configuration with $K = 5/2$. The energies are plotted relative to the $11/2^-$ state of Band 1.

in ^{133,135}Pm and finally backbend in ^{137,139}Pm were well established in earlier studies [16,20,29], reflecting a common trend of stronger quasiparticle interaction in lighter odd-A Pm isotopes.

In Band 1, a smooth upbend is observed from the alignment plot shown in Fig. 5 and it undergoes two crossings as can be noted from the results of Ref. [20]. The first AB crossing

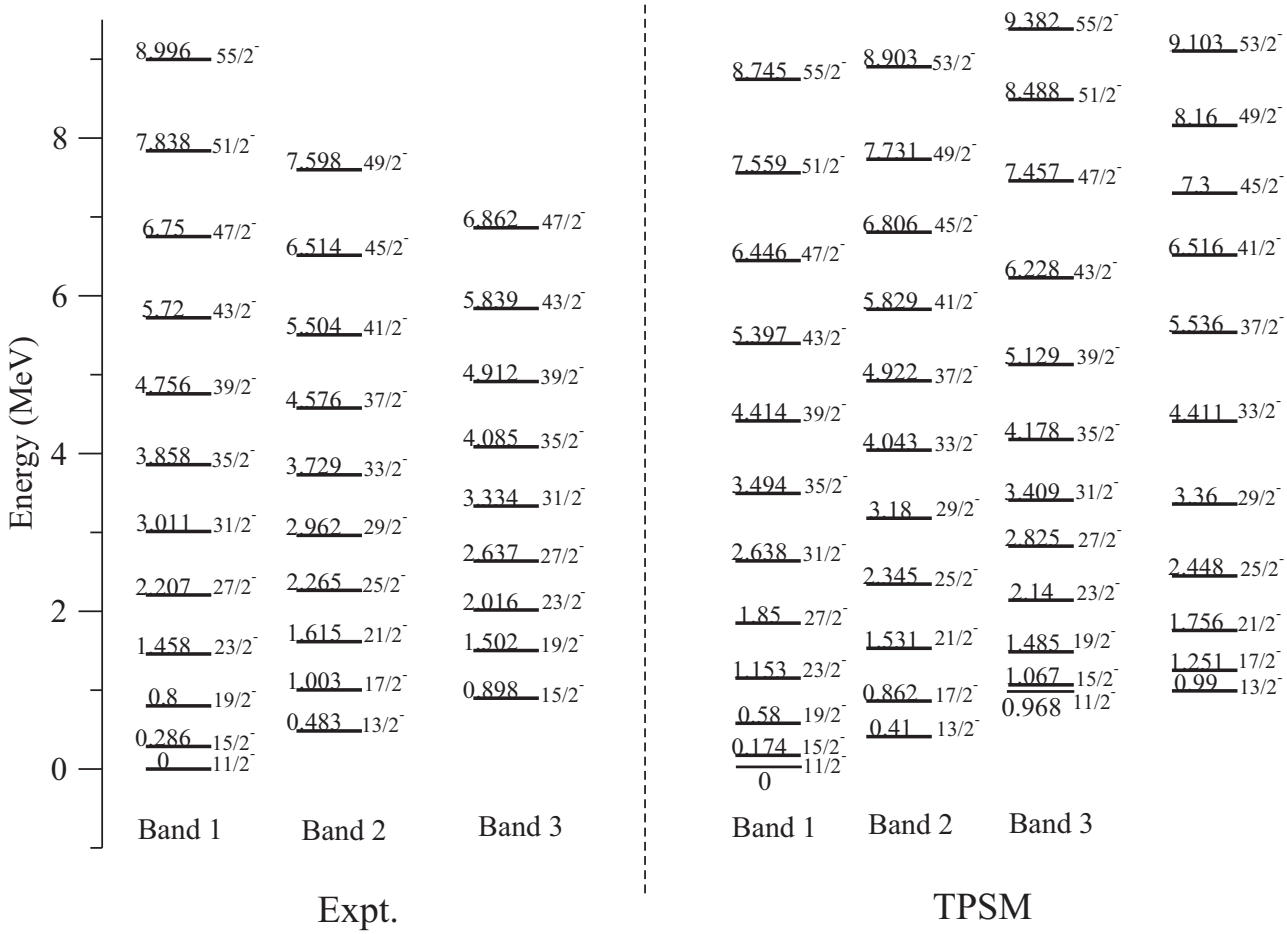

FIG. 7. Comparison of experimentally observed level energies of negative-parity Band 1, Band 2, and Band 3 with the values obtained from TPSM calculations. The energies are given relative to the $11/2^-$ state of Band 1.

in an odd-proton system is blocked in the proton sector and the crossing observed at $\hbar\omega = 0.43$ MeV is attributed to the BC crossing. Since ^{135}Pm nucleus is γ soft, both proton and neutron alignments are possible with opposite driving forces at the same frequency [36]. The cranked shell model suggests the proton pair alignment [16] which is also the case in ^{133}Pr isotone [8]. On the other hand, the extended total Routhian surface calculations demonstrated that both the neutron and proton pairs have almost equal contributions to the first observed crossing with neutron crossing occurring at lower frequency [20]. Therefore, it becomes a complex band-crossing phenomenon which can lead to interesting band structures. Such a prediction motivates to further probe the band-crossing mechanism using new experimental data as well as theoretical model calculations. For the case of Band 3, a backbend is observed at $\hbar\omega = 0.30$ MeV from the alignment plot in Fig. 5, suggesting the role of different quasiparticle configurations involved in this band crossing. A similar band was observed in ^{133}Pm (Band 7 in Ref. [15]), but the detailed explanation was not given. This alludes to the possibility of a delicate competition between the alignment of proton and neutron pairs involved at high spin.

The experimental $B(E2)$ transition strengths for various spin values ($I^\pi = 23/2^-$ to $39/2^-$) are given in Table II. This observation is providing new information of evolution of collectivity along the yrast band and is different from the previous results which indicated a steeper decline in $B(E2)$ values at a very low spin [4]. The present experimental values suggest a moderate increase in collectivity until the first band crossing. The slight reduction thereafter is due to the first crossing of three-quasiparticle band. It is worth mentioning that an almost constant quadrupole moment after the first crossing in ^{133}Pm was reported in [15] which indicates a stronger interaction among the bands leading to no apparent change in collectivity.

A. Triaxial projected shell-model approach

In recent years, TPSM approach has been demonstrated to reproduce the high-spin properties of deformed nuclei quite satisfactorily [37]. In this model, the odd-proton systems have been studied with the model space of one-proton and one-proton coupled to two-neutron quasiparticle states. In order to investigate the high-spin states of ^{135}Pm observed in the present work, the basis space has been generalized to include both three-proton, and three-proton coupled to two-neutron quasiparticle states. The complete basis space in the gener-

alized approach is given by:

$$\begin{aligned} \hat{P}^I_{MK}\, a^\dagger_{\pi_1} \mid \Phi > , \\ \hat{P}^I_{MK}\, a^\dagger_{\pi_1} a^\dagger_{\nu_1} a^\dagger_{\nu_2} \mid \Phi > , \\ \hat{P}^I_{MK}\, a^\dagger_{\pi_1} a^\dagger_{\pi_2} a^\dagger_{\pi_3} \mid \Phi > , \\ \hat{P}^I_{MK}\, a^\dagger_{\pi_1} a^\dagger_{\pi_2} a^\dagger_{\pi_3} a^\dagger_{\nu_1} a^\dagger_{\nu_2} \mid \Phi > , \end{aligned} \tag{2}$$

where $\hat{P}^I_{MK}$ is the three-dimensional angular-momentum-projection operator [38]. The triaxial quasiparticle (qp) vacuum $|\Phi>$ in Eq. (2) is determined through diagonalization of the deformed Nilsson Hamiltonian and a subsequent BCS calculations. This provides the triaxial qp basis for the calculations. In the present work, we have compared the experimental band structure and transition rates of ^{135}Pm with the numerical results obtained using the TPSM approach. The details of this formalism for odd-A nuclei can be found in Ref. [39] which has been successful in describing the high-spin states in ^{103,105}Rh [40]. TPSM provided a theoretical understanding of the first 2γ band observed in odd-A nucleus [41]. In case of ^{135}Pm, same prescription has been followed where quasiparticle states were generated by solving the triaxial Nilsson and pairing (monopole and quadrupole terms) Hamiltonian in the BCS approximation. The Nilsson potential with the deformation parameters $\epsilon = 0.23$ and $\epsilon' = 0.11$ have been used for ^{135}Pm. The configuration space consists of $N = 3, 4, 5$ major shells for both neutrons and protons. About 40 lowest K bands were obtained through angular momentum projection within the energy window of 2.5 MeV. These projected bands (basis states) were employed to diagonalize the shell-model Hamiltonian consisting of pairing and quadrupole-quadrupole interaction terms. The interaction strengths used in the present calculations were the same as those used in the previous studies [39,40].

The band structures obtained from the angular-momentum projection of lowest quasiparticle states in the vicinity of the Fermi surface are shown in Fig. 6. This figure depicts projected bands before band mixing and plays an important role to unravel the band crossing features. The lowest band with large signature splitting is the projected state with $K = 3/2$ and originates from the proton occupying the intruder orbital, $1h_{11/2}$. This band is noted to be crossed at $I = 31/2$ by a projected band having three-proton quasiparticle structure with $K = 3/2$. It is also evident from the figure that the projected three-quasiparticle band with one-proton coupled to two-neutrons also becomes favored in energy and crosses the one-proton configuration at about $I = 35/2$. This almost simultaneous crossing of two bands with different neutron and proton configurations is expected to lead to the forking of the yrast band into two s bands as observed in some even-even isotopes. This feature shall be discussed in detail when comparing with the experimental data. Further, the five-quasiparticle configuration with three-protons coupled to two-neutrons crosses the three-proton configuration at $I = 47/2$. It is noted from Fig. 6 that there are many band structures in the vicinity of the yrast line and it is expected that mixing among these bands shall play an important role in the description of the near-yrast spectroscopy.

The bands for each angular momentum from the intrinsic states about the Fermi surface, about 40 in number, are used to diagonalize the shell-model Hamiltonian consisting of pairing plus quadrupole-quadrupole interaction [42]. The calculated lowest band structures after diagonalization are displayed in Fig. 7 along with the known experimental data. It is evident from the figure that experimental energies are reproduced within few hundred keV for most of the states. In order to examine the structural evolution of the observed band structures with spin, the probabilities within the wave functions are depicted in Fig. 8. Band 1 and Band 2 are predominantly composed of one-quasiparticle states up to $I = 27/2$ and above this spin value, it is noted that three-quasiparticle states, both 3π and $1\pi 2\nu$, become increasingly dominant with spin. In the spin regime, between $I = 35/2$ and $43/2$ for $\alpha = -1/2$ and between $I = 37/2$ and $45/2$ for $\alpha = 1/2$, Band 1 and Band 2 have essentially three-quasiparticle structure with 3π component slightly more than that of $1\pi 2\nu$. The bands have $3\pi 2\nu$ five-quasiparticle structure above $I = 45/2$.

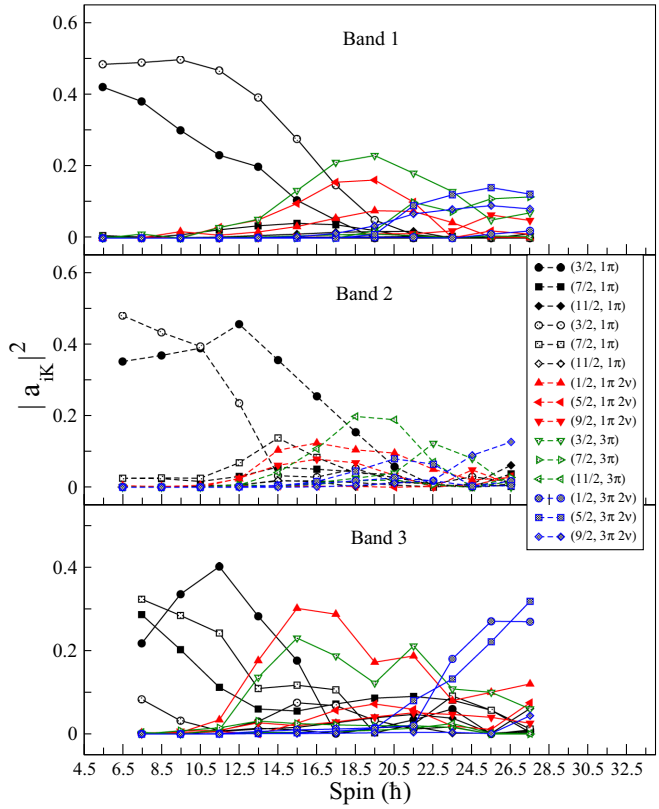

FIG. 8. Probability of various projected K configurations in the wave functions of the observed Band 1, Band 2, and Band 3 in ^{135}Pm. Only the lowest projected K configurations in the wave functions of bands are shown. The solid curves represent the $\alpha = -1/2$ states with same legend symbols and quasiparticle states as that of $\alpha = +1/2$ states plotted in dashed curves. Legends for only $\alpha = +1/2$ states are shown for better visual clarity.

Due to large number of bands present in the crossing region, it is expected that band crossings will be smooth. This smooth crossing behavior is evident in the alignment plots of Figs. 9(a), 9(b) and 9(c) shown in the left panel of the figure, in which i_x depicted a smoothly increasing trend with spin for the observed three bands. The TPSM calculated i_x are

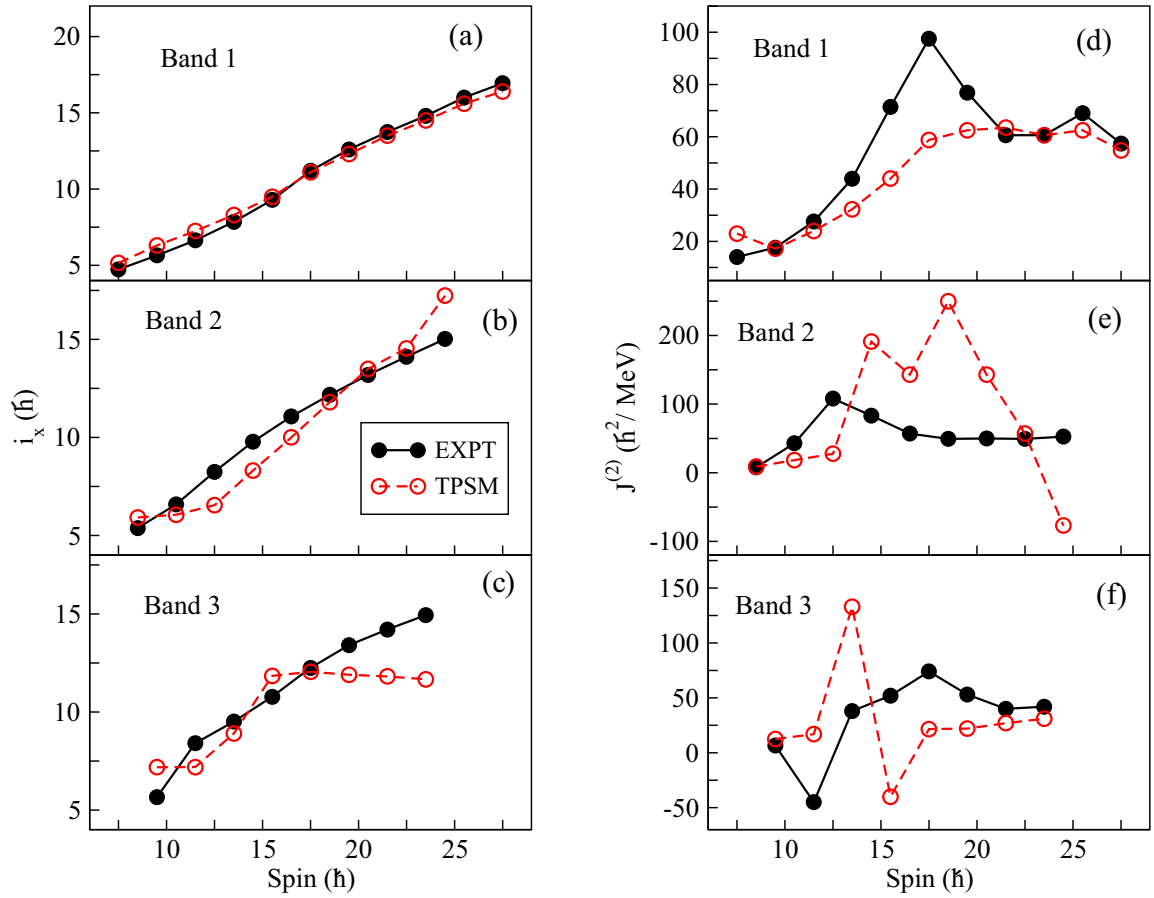

FIG. 9. Comparison between experimental and theoretical (TPSM) values of alignment (i_x) and dynamic moment of inertia ($J^{(2)}$) as a function of spin ($\hbar$) for the quadrupole negative-parity bands in ^{135}Pm. The left panel consists of i_x for (a) Band 1, (b) Band 2, and (c) Band 3 while the right panel contains ($J^{(2)}$) for (d) Band 1, (e) Band 2, and (f) Band 3.

in good agreement with those extracted from the observed quantities, except that at high-spin TPSM results for Band 3, depict saturation of the alignment while the measured i_x shows increasing trend. The dynamic moment of inertia, $J^{(2)}$, shown in the right panel of Fig. 9, which is very sensitive to band crossing, depict two upbends in the measured quantity for Band 1, one at around $I = 35/2$ and the other at $I = 51/2$. The calculated $J^{(2)}$ from the TPSM shows smoother upbend as compared to the corresponding experimental values which indicates that the interaction between the bands is overestimated in the model. It is evident from the band diagram in Fig. 6 and also from the wave functions, shown in Fig. 8, that the first crossing ($\hbar\omega = 0.43$ MeV, $I = 35/2$) is due to the crossing of three-quasiparticles, which is a mixture of 3π and $1\pi 2\nu$. The second crossing ($\hbar\omega = 0.54$ MeV, $I = 51/2$) is due to the crossing of five-quasiparticles having $3\pi 2\nu$ configuration. In the cranked shell-model analysis presented in Ref. [20], the first crossing has been predicted to have contributions from both protons and neutrons and agrees with the TPSM results. However, the five-quasiparticle crossing in CSM is predicted at $\hbar\omega = 0.8$ MeV, which is at variance with the experimental as well as TPSM results.

TPSM results of $J^{(2)}$ are somewhat in disagreement with the measured values for Band 2 and Band 3. As $J^{(2)}$ is a very sensitive quantity, small changes in pairing and deformation for these bands could contribute to these differences. It needs to be mentioned that in TPSM approach, the mean field is held fixed for all the spin states and excitation energies. It is known from microscopic studies that mean field can change with spin and excitation energy.

TPSM results also provide a possible explanation of the appearance of Band 3 in the observed data. The wave function of Band 3 is displayed in Fig. 8. The structure is very similar to what is observed for the Band 1 and Band 2, except that neutron and proton contributions to the probabilities are reversed. In the absence of the interaction among the bands, the yrast band after the first crossing will have 3π character and Band 3 will have $1\pi 2\nu$ structure. This is because in the band diagram of Fig. 6, 3π and $1\pi 2\nu$ configurations almost simultaneously cross the yrast band. This crossing of the yrast band with two s bands has been observed in some of the even-even systems [43,44] where proton and neutron Fermi surfaces are close in the energy. Such a crossing involving two s bands is usually not expected in an odd-A nucleus with the two-particles aligning in the same orbital as that of the odd-particle. Normally, in odd-mass nuclei, one-proton/neutron quasiparticle state is occupied by the last proton/neutron and the corresponding proton/neutron AB crossing is not possible as in even-even systems. The first crossing is normally observed due to the crossing of the even components of neutrons/protons. There-

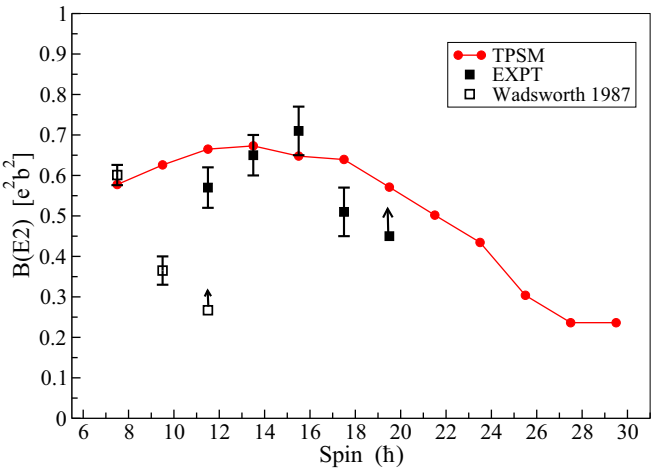

FIG. 10. Experimentally measured values of $B(E2)$ transition strengths are compared with the theoretical values calculated within TPSM formalism. The filled squares correspond to the experimental $B(E2)$ values. Previously reported values, shown in open squares, are adapted from Ref. [4].

fore, the simultaneous crossing of neutron and proton *s* bands with the yrast band is not expected in an odd system due to the blocking argument. However, in the present system of odd-proton ^{135}Pm isotope, we observe such a band crossing phenomenon that we consider to be quite rare. It is very likely that there might be several other odd-*A* nuclei where such band structures exist and need to be probed in the way ^{135}Pm has been investigated in the present work.

We have also calculated the electromagnetic transitions using the TPSM wave functions with the effective charges of 1.6*e* for protons and 0.6*e* for neutrons. The details were already discussed in our work [45] and shall not be repeated here. The calculated $B(E2)$ transition probabilities for Band 1 are plotted in Fig. 10 along with the present experimental values and previous results for lower-spin states [4]. The previously reported $B(E2)$ value for the $I^\pi = 15/2^-$ state indicated a moderate deformation with ϵ_2 around 0.23 for ^{135}Pm [4] and this $B(E2)$ value is well reproduced by the current TPSM results. However, the sharp drop in the $B(E2)$ values above $I^\pi = 15/2^-$ observed in the previous work [4] has not been explained by the current calculations. From the present lifetime measurements, the B($E2$) values for higher-spin states remain constant and show a gradual drop at $I^\pi = 35/2^-$. The calculated $B(E2)$ values explain this feature. Beyond $I = 35/2$, a smooth drop is observed. Normally, at the band crossing a rapid change in the transition probability is expected, however, due to large mixing among different states in the band crossing region, a smoother drop is noted in the TPSM calculations. It is evident from Fig. 10 that TPSM results are in good agreement with the available measured values. This $B(E2)$ reduction is from changes in the structure of the wave functions as different quasiparticle states continuously enter into the yrast region with increasing spin as depicted in Fig. 8. It is interesting to note that a pronounced decrease in the high-spin $B(E2)$ of ^{134}Nd [46], an isotone of ^{135}Pm, is predicted, which suggests reduction of collectivity at very high spins because of increased level density and complex band mixing.

V. SUMMARY

Spectroscopic investigations have been performed to study the structure of three negative-parity bands in odd-proton ^{135}Pm nucleus. The $B(E2)$ transition strengths extracted from the measurements of level lifetimes using DSAM indicate loss of collectivity for the yrast band at higher spin. The multiple band structures observed have been interpreted in the framework of TPSM. The calculations provide a possible explanation of the three bands in terms of two *s* bands crossing the yrast band at similar spin values and give a new insight about the subtle alignment mechanism in ^{135}Pm. The variations of the alignment and dynamic moment of inertia with spin for the yrast band have been nicely explained through this rare crossing of two *s* bands in an odd-*A* nucleus. In addition, the band crossing dynamics explains the gradual decrease in $B(E2)$ values of yrast states.

ACKNOWLEDGMENTS

Authors are grateful to the staff at TIFR-BARC Pelletron Linac Facility for providing a good-quality beam and smooth operation of the accelerator for the entire duration of the experiment. The help and cooperation from B. Naidu, S. Jadhav, Abraham T. Vazhappilly, and R. Donthi for setting up the experimental apparatus is acknowledged. We thank Prof. Mark Riley for useful discussions during the FIG-2018 conference, including on the FSU work on this nucleus. This work is supported by the Department of Atomic Energy, Government of India (Project Identification Code: 12-R&D-TFR-5.02-0200); the Department of Science and Technology, Government of India (Grant No. IR/S2/PF-03/2003-II); and the U.S. National Science Foundation (Grant No. PHY-1713857). The financial support provided by DST for Project No. CRG/2019/004960 is gratefully acknowledged by J.A.S. and G.H.B.

[1] R. W. Laird, F. G. Kondev, M. A. Riley, D. E. Archer, T. B. Brown, R. M. Clark *et al.*, Phys. Rev. Lett. **88**, 152501 (2002).
[2] C. J. Lister *et al.*, Phys. Rev. Lett. **55**, 810 (1985).
[3] F. S. Babra, R. Palit, S. Rajbanshi, S. Jehangir, B. Das, G. H. Bhat, J. A. Sheikh, S. Biswas, U. Garg, Md. S. R. Laskar, C. Palshetkar, S. Saha, J. Sethi, and P. Singh, Phys. Rev. C **100**, 054308 (2019).
[4] R. Wadsworth, J. M. O'Donnell, D. L. Watson, P. J. Nolan, A. Kirwan, P. J. Bishop, M. J. Godfrey, D. J. Thornley, and D. J. G. Love, J. Phys. G **13**, 205 (1987).
[5] P. J. Smith, D. J. Unwin, A. Kirwan, D. J. G. Love, A. H. Nelson, P. J. Nolan, and D. M. Todd, J. Phys. G **11**, 1271 (1985).
[6] L. Hildingsson, C. W. Beausang, D. B. Fossan, R. Ma, E. S. Paul, W. F. Piel, Jr., and N. Xu, Phys. Rev. C **39**, 471 (1989).

[7] N. Xu, C. W. Beausang, R. Ma, E. S. Paul, W. F. Piel, Jr., D. B. Fossan, and L. Hildingsson, Phys. Rev. C **39**, 1799 (1989).

[8] L. Hildingsson, C. W. Beausang, D. B. Fossan, and W. F. Piel, Jr., Phys. Rev. C **33**, 2200 (1986).

[9] T. M. Semkow, D. G. Sarantites, K. Honkanen, V. Abenante, L. A. Adler, C. Baktash, N. R. Johnson, I. Y. Lee, M. Oshima, Y. Schutz, Y. S. Chen, J. X. Saladin, C. Y. Chen, O. Dietzsch, A. J. Larabee, L. L. Riedinger, and H. C. Griffin, Phys. Rev. C **34**, 523 (1986).

[10] N. Xu, C. W. Beausang, J. R. Hughes, Y. Liang, R. Ma, E. S. Paul, W. F. Piel, Jr., S. Shi, and D. B. Fossan, Phys. Rev. C **43**, 2189 (1991).

[11] P. Vaska, C. W. Beausang, D. B. Fossan, J. R. Hughes, R. Ma, E. S. Paul, R. J. Poynter, P. H. Regan, R. Wadsworth, S. A. Forbes, S. M. Mullins, and P. J. Nolan, Phys. Rev. C **52**, 1270 (1995).

[12] A. Dhal, R. K. Sinha, L. Chaturvedi, P. Agarwal, S. Kumar, A. K. Jain *et al.*, Phys. Rev. C **80**, 014320 (2009).

[13] N. T. Zhang *et al.*, Phys. Rev. C **84**, 057302 (2011).

[14] P. K. Weng *et al.*, Phys. Rev. C **47**, 1428 (1993).

[15] A. Galindo-Uribarri, D. Ward, H. R. Andrews, G. C. Ball, D. C. Radford, V. P. Janzen, S. M. Mullins, J. C. Waddington, A. V. Afanasjev, and I. Ragnarsson, Phys. Rev. C **54**, 1057 (1996).

[16] C. W. Beausang, L. Hildingsson, E. S. Paul, W. F. Piel, Jr., P. K. Weng, N. Xu, and D. B. Fossan, Phys. Rev. C **36**, 602 (1987).

[17] J. T. Matta, U. Garg, W. Li, S. Frauendorf, A. D. Ayangeakaa, D. Patel *et al.*, Phys. Rev. Lett. **114**, 082501 (2015).

[18] P. Möller, R. Bengtsson, B. G. Carlsson, P. Olivius, and T. Ichikawa, Phys. Rev. Lett. **97**, 162502 (2006).

[19] G. A. Leander and P. Möller, Phys. Lett. B **110**, 17 (1982).

[20] C. M. Parry *et al.*, Phys. Rev. C **57**, 2215 (1998).

[21] H. Tan *et al.*, in *Proceedings of the IEEE Nuclear Science Symposium and Medical Imaging Conference (NSS/MIC'08)* (IEEE, Los Alamitos, CA, 2009), p. 2471.

[22] R. Palit, S. Saha, J. Sethi, T. Trivedi, S. Sharma, B. S. Naidu, S. Jadhav, R. Donthi, P. B. Chavan, H. Tan *et al.*, Nucl. Instrum. Methods A **680**, 90 (2012).

[23] D. C. Radford, Nucl. Instrum. Methods A **361**, 297 (1995).

[24] A. Krämer-Flecken, T. Morek, R. M. Lieder, W. Gast, G. Hebbinghaus, H. M. Jäger, and W. Urban, Nucl. Instrum. Methods A **275**, 333 (1989).

[25] K. Starosta, T. Morek, C. Droste, S. G. Rohozinski, J. Srebrny, A. Wierzchucka, M. Bergström, B. Herskind, E. Melby, T. Czosnyka *et al.*, Nucl. Instrum. Methods A **423**, 16 (1999).

[26] R. Palit, H. C. Jain, P. K. Joshi, S. Nagaraj, B. V. T. Rao, S. N. Chintalapudi, and S. S. Ghugre, Pramana **54**, 347 (2000).

[27] P. M. Jones *et al.*, Nucl. Instrum. Methods A **362**, 556 (1995).

[28] Y. Zheng, G. de France, E. Clement, A. Dijon, B. Cederwall, R. Wadsworth *et al.*, Phys. Rev. C **87**, 044328 (2013).

[29] W. Pei-Kun, Y. Guan-Jun, Z. Zhan-Jun, L. Sheng-Gang, W. Shu-Xian, L. Guang-Sheng, D. Zheng-Yu, Y. Chun-Xiang, P. Zhao-Hua, L. Xiang-An, W. Xiao-Guang, and P. Yun-Weit, Chin. Phys. Lett. **18**, 30 (2001).

[30] N. R. Johnson, J. C. Wells, Y. Akovali, C. Baktash, R. Bengtsson, M. J. Brinkman, D. M. Cullen, C. J. Gross, H.-Q. Jin, I.-Y. Lee, A. O. Macchiavelli, F. K. McGowan, W. T. Milner, and C.-H. Yu, Phys. Rev. C **55**, 652 (1997).

[31] L. C. Northcliffe and R. F. Schilling, Nucl. Data Tables A **7**, 233 (1970).

[32] S. Rajbanshi, A. Bisoi, S. Nag, S. Saha, J. Sethi, T. Trivedi, T. Bhattacharjee, S. Bhattacharyya, S. Chattopadhyay, G. Gangopadhyay, G. Mukherjee, R. Palit, R. Raut, M. Saha Sarkar, A. K. Singh, and A. Goswami, Phys. Rev. C **89**, 014315 (2014).

[33] C. J. Chiara, S. J. Asztalos, B. Busse, R. M. Clark, M. Cromaz, M. A. Deleplanque, R. M. Diamond, P. Fallon, D. B. Fossan, D. G. Jenkins, S. Juutinen, N. S. Kelsall, R. Krucken, G. J. Lane, I. Y. Lee, A. O. Macchiavelli, R. W. MacLeod, G. Schmid, J. M. Sears, J. F. Smith, F. S. Stephens, K. Vetter, R. Wadsworth, and S. Frauendorf, Phys. Rev. C **61**, 034318 (2000).

[34] A. D. Ayangeakaa *et al.*, Phys. Rev. Lett. **110**, 102501 (2013).

[35] A. Dhal *et al.*, Eur. Phys. J. A **48**, 28 (2012).

[36] R. Wadsworth, J. M. O'Donnell, D. L. Watson, P. J. Nolan, A. Kirwan, P. J. Bishop, M. J. Godfrey, D. J. Thornley and D. J. G. Love, J. Phys. G: Nucl. Phys. **14**, 239 (1988).

[37] J. A. Sheikh and K. Hara, Phys. Rev. Lett. **82**, 3968 (1999).

[38] P. Ring and P. Schuck, *The Nuclear Many-Body Problem* (Springer-Verlag, New York, 1980).

[39] G. H. Bhat, J. A. Sheikh, and R. Palit, Phys. Lett. B **707**, 250 (2012).

[40] G. H. Bhat, J. A. Sheikh, W. A. Dar, S. Jehangir, R. Palit, and P. A. Ganai, Phys. Lett. B **738**, 218 (2014).

[41] J. A. Sheikh, G. H. Bhat, Y. Sun, and R. Palit, Phys. Lett. B **688**, 305 (2010).

[42] K. Hara and Y. Sun, Int. J. Mod. Phys. E **4**, 637 (1995).

[43] M. Kumar Raju, P. V. Madhusudhana Rao, S. Muralithar, R. P. Singh, G. H. Bhat, J. A. Sheikh, S. K. Tandel, P. Sugathan, T. Seshi Reddy, B. V. Thirumala Rao, and R. K. Bhowmik, Phys. Rev. C **93**, 034317 (2016).

[44] R. Wyss, A. Granderath, R. Bengtsson, P. von Brentano, A. Dewald, A. Gelberg, A. Gizon, J. Gizon, S. Harissopulos, A. Johnson, W. Lieberz, W. Nazarewicz, J. Nyberg, and K. Schiffer, Nucl. Phys. A **505**, 337 (1989).

[45] J. A. Sheikh, G. H. Bhat, W. A. Dar, S. Jehangir, and P. A Ganai, Phys. Scr. **91**, 063015 (2016).

[46] Long-Jun Wang, Y. Sun, T. Mizusaki, M. Oi, and S. K. Ghorui, Phys. Rev. C **93**, 034322 (2016).